

Computer Methods in Biomechanics and Biomedical Engineering

ISSN: (Print) (Online) Journal homepage: <https://www.tandfonline.com/loi/gcmb20>

Efficacy of quantifying marker-cluster rigidity in a multi-segment foot model: a Monte-Carlo based global sensitivity analysis and regression model

Po-Hsiang Chan, Julie Stebbins & Amy B. Zavatsky

To cite this article: Po-Hsiang Chan, Julie Stebbins & Amy B. Zavatsky (2021): Efficacy of quantifying marker-cluster rigidity in a multi-segment foot model: a Monte-Carlo based global sensitivity analysis and regression model, Computer Methods in Biomechanics and Biomedical Engineering, DOI: [10.1080/10255842.2021.1954170](https://doi.org/10.1080/10255842.2021.1954170)

To link to this article: <https://doi.org/10.1080/10255842.2021.1954170>



© 2021 The Author(s). Published by Informa UK Limited, trading as Taylor & Francis Group



Published online: 22 Jul 2021.



Submit your article to this journal [↗](#)



Article views: 133



View related articles [↗](#)



View Crossmark data [↗](#)

Efficacy of quantifying marker-cluster rigidity in a multi-segment foot model: a Monte-Carlo based global sensitivity analysis and regression model

Po-Hsiang Chan^a, Julie Stebbins^b and Amy B. Zavatsky^a

^aDepartment of Engineering Science, University of Oxford, Oxford, UK; ^bOxford Gait Laboratory, Nuffield Orthopaedic Centre NHS Trust, Oxford, UK

ABSTRACT

Marker-based clinical gait analysis and multi-segment foot models (MSFM) have been successfully used for the diagnosis and clinical management of various lower limb disorders. The accuracy and validity of the kinematics measured depend on the design of the model, as well as on the adherence to its inherent rigid body assumption. This study applies a Monte-Carlo based global sensitivity analysis to evaluate the efficacy of using 'rigid body error (σ_{RBE})' in quantifying the rigidity of a MSFM marker-cluster. A regression model is proposed. It is concluded that σ_{RBE} is effective in quantifying rigidity.

ARTICLE HISTORY

Received 30 July 2020
Accepted 7 July 2021

KEYWORDS

Global sensitivity analysis; rigidity; Procrustes; foot model; Monte-Carlo; marker-cluster

1. Introduction

Stereophotogrammetry-based clinical gait analysis has been implemented in biomechanical laboratories and hospitals all over the world to analyse the condition of various pathologies, including foot deformities such as those seen in cerebral palsy and clubfoot (Theologis and Stebbins, 2010), arthritis (Turner and Woodburn, 2008), diabetic gait (Sawacha et al., 2009), and many more (Leardini et al., 2019). In a clinical gait laboratory, multi-segment foot models (MSFMs) have been used to capture quantitative information about human motion to help guide diagnosis, treatment planning, and the assessment of surgical outcome (Rankine et al., 2008; Deschamps et al., 2011; Leardini et al., 2019). The methodology generally involves dividing the lower-limb into multiple rigid body segments, typically the pelvis, thigh, shank, and foot, and tracking them using markers (or markers on rigid bases) attached to the skin. Kinematics of the joints can then be computed by describing the orientation of a distal segment with reference to a proximal segment. Markers are also used to track bony landmarks to facilitate the computation of biomechanical parameters or clinically relevant information, such as the foot arch height or the first metatarsophalangeal angle. Both the segment definition (segmentation and marker placement) and the kinematic description of each model differ largely

depending on the clinical need, technology limitation, and the designer's criteria.

Despite the success of using MSFMs in the clinical setting and for biomechanical research, the inherent rigid body assumption can cause misinterpretations due to the differences in the motion measured from the model and the actual anatomical motion. From a methodological perspective, a rigid segment representing multiple bones (e.g. mid-foot and forefoot) may not be appropriate, potentially losing or misrepresenting important clinical information (Nester et al., 2010; DiLiberto et al., 2015; Pothrat et al., 2015). This is particularly true for the forefoot segment, with a number of studies questioning the validity of assuming a single segment forefoot (Wolf et al., 2008; Rouhani et al., 2011; Chan et al., 2019) and a review confirming the lack of consensus on how it is currently tracked (Rankine et al., 2008). Lower-limb segments that may reasonably be assumed to act as a single bony entity such as the thigh and pelvis also are liable to soft tissue artefacts (STA), where movement of the soft tissues causes the skin-attached markers to move relative to the underlying bone (Leardini et al., 2005). While the assumption of rigidity in MSFM segments greatly simplifies the computation and allows for easy implementation, it is essential to understand and quantify the deformations of groups of individual tracking

CONTACT Amy B. Zavatsky  amy.zavatsky@eng.ox.ac.uk

© 2021 The Author(s). Published by Informa UK Limited, trading as Taylor & Francis Group

This is an Open Access article distributed under the terms of the Creative Commons Attribution-NonCommercial-NoDerivatives License (<http://creativecommons.org/licenses/by-nc-nd/4.0/>), which permits non-commercial re-use, distribution, and reproduction in any medium, provided the original work is properly cited, and is not altered, transformed, or built upon in any way.

markers (or ‘marker-clusters’) in order to guide segmentation, to design better MSFM models, and to minimise kinematic errors due to STA.

Deformation can be easily quantified using standard measures from classical mechanics, such as the change in Euclidean distance or engineering strain. However, the deformation magnitude is different depending on the reference point chosen. Therefore, these measures are unsuitable in the case of a MSFM where all the markers can act as a reference point, thus giving different results. An alternative method of quantifying non-rigid motion is by computing the rigid body error, σ_{RBE} (van den Bogert et al., 1994). σ_{RBE} originates from the computation of residuals from the Procrustes analysis. It represents the difference between two geometries (here, of the marker-clusters). In the past, studies have utilised residuals to quantify the non-rigid motion of the soft tissue artefact (van den Bogert et al., 1994; Grimpampi et al., 2014), minimise rotation error (Leitch et al., 2010), and quantify MSFM segment rigidity (Spoor and Veldpaus, 1980; Bruening et al., 2012; Chan et al., 2019), but they have yet to show that it is an appropriate representation of the actual movement. To our knowledge, there is currently no study assessing the efficacy and validity of using the σ_{RBE} to quantify rigidity or deformation.

Therefore, the purpose of this study was to determine whether σ_{RBE} is a suitable measure to quantify the rigidity of a generic MSFM segment, through assessing how variations in the deformation of marker-clusters with different arrangements could influence the computation of the σ_{RBE} . This problem can be treated similar to a mathematical model where the contribution of each input to output variable (here, the σ_{RBE}) can be examined through a global sensitivity analysis (GSA), uncertainty analysis (UA), and regression analysis (RA) (Saltelli et al., 2007). In this study, GSA is used to investigate the relationship between σ_{RBE} and its input variables; UA to validate the generated input variables and provide an estimation of the σ_{RBE} ; and RA to confirm the relationship between the magnitude of deformation and the σ_{RBE} .

2. Methods

2.1. Rigid body error algorithm

Rigid body error (σ_{RBE}) originated from solving the orthogonal Procrustes problem (Schönemann, 1966). Proposed by van den Bogert (van den Bogert et al., 1994), the σ_{RBE} is computed as:

$$\sigma_{RBE} = \sqrt{\frac{1}{3n-6} \| [T][A] - [B] \|^2} \quad (1)$$

where n is the number of markers, $[A]$ is the reference configuration of the marker-cluster, $[B]$ is the deformed configuration of the marker-cluster, and $[T]$ the orthogonal transformation matrix for which the equation $\| [T][A] - [B] \|^2$ is minimised. The minimisation problem is also known as the Procrustes problem, where the algorithm attempts to find the transformation matrix that best describes the movement from $[A]$ to $[B]$. A number of papers have discussed and improved the solution to the orthogonal Procrustes problem (Green, 1951; Schönemann, 1966; Hanson and Norris, 1981; Söderkvist and Wedin, 1994, 1993). One of the solutions that utilises singular value decomposition, proposed by Söderkvist and Wedin (1993), showed more stability and can be easily implemented in programming for various applications, including human motion analysis. In this study, $[T]$ will be determined using the algorithm proposed by Söderkvist and Wedin (1993).

2.2. Monte-Carlo simulation

The experiment was designed such that N number of randomly generated marker-cluster configurations $[A]$ were subjected to a random rotation $[R]$ and deformation $[\delta D]$, where the mismatch between the shape of the original configuration $[A]$ and the deformed configuration $[B]$ can be quantified using σ_{RBE} . A GSA was applied to evaluate the relationship between $[\delta D]$ and σ_{RBE} , and to assess which other variables also contribute to or associate with the variation of the σ_{RBE} . All computations were completed using MATLAB (vR2017a, MathWorks Inc., Natick, USA).

The Monte-Carlo based technique provides direct estimation of the mean and standard deviation required to perform uncertainty analysis, as well as the sensitivity indices based on various regression coefficients. The major drawback for the Monte-Carlo method is the computation cost and the requirement of a large sample size (Iooss and Lemaitre, 2015). Therefore, a convergence assessment was also conducted in this study (see Appendix A). The minimum number of samples required to reach convergence was 3197, and therefore a sample size of 5000 was used for the calculations. This reduced the computation cost by avoiding an unnecessarily large sample size and ensured the credibility of the sensitivity parameters.

Table 1 outlines the computation steps for generating the Monte-Carlo samples. First, the three inputs ($[A_N]$, $[R_N]$, and $[\delta D_N]$) were randomised based on pre-

Table 1. Summary of Monte-Carlo computation steps and the computation of all outputs.

Steps	Mathematical representations
Generating Monte-Carlo samples	
1. Generate random marker configuration $[A]$	$[A]$, where $a_{ij} \in [-250, 250]$
2. Apply a random rotation $[R]$	$[R][A]$, where $\beta, \gamma \in [0, 2\pi]; x \in [0, 1]$
3. Add a random deviation $[\delta D]$	$[B] = [R][A] + [\delta D]$, where $\delta d_{1,1} \in [-50, 50]$
Compute best fitting transformation matrix and all the other outputs	
4. Compute transformation matrix $[T]$	$[T]$, where $\min\ [T][A] - [B]\ $ describes the transformation from $[A]$ to $[B]$
5. Compute rigid body error σ_{RBE}	$\sigma_{RBE} = \sqrt{\frac{1}{3n-6}}\ [T][A] - [B]\ $
6. Compute rotation error R_{err} based on the difference between the $[R]$ and $[T]$	$R_{err} = \left\ \begin{bmatrix} R_{11} & R_{12} & R_{13} & t_x \\ R_{21} & R_{22} & R_{23} & t_y \\ R_{31} & R_{32} & R_{33} & t_z \\ 0 & 0 & 0 & 1 \end{bmatrix} - T \right\ $ <p>Where the translation vector $t = (t_x, t_y, t_z) = (000)$ since no translation was applied.</p>
7. Compute condition number kA	$kA = (\sigma_2^2 + \sigma_3^2)^{-1/2}$, where σ_2 and σ_3 are the two smallest singular values of $[A]$
8. Compute segment size S	$S = \frac{1}{n} \sum_{i=1}^n [a]_{ij} - [\bar{a}] $, where $[\bar{a}] = \frac{1}{n} \sum_{i=1}^n a_{ij}$, the geometric centroid of all the markers considered, and a_{ij} the coordinates of individual markers. (Here $n = 4$ markers)

Note that the computed $[T]$ in step 6 may contain non-zero t for the best-fit transformation.

defined ranges. $[A_N]$ is a 4×3 matrix that simulates a four marker cluster on an MSFM segment (one more than the minimum of three tracking markers). Each matrix element, a_{ij} , where the lower case letter with subscript ij refers to the entry of the matrix that represents the i^{th} marker and j the axes of the Cartesian coordinates of the marker ($j \in (x, y, z)$), was sampled from a uniform distribution over $[-250, 250]$ mm. This allows the marker-cluster to take all possible arrangements within the sampling region of a 500 mm^3 cube, as a typical MSFM segment size falls within this volume.

Next, $[A]$ was randomly rotated about the origin based on the rotation matrix generating algorithm described by Arvo (1992). This method utilises a reflection after the first rotation to produce a truly random rotation. It requires the input of two angles ($\beta_N, \gamma_N \in [0, 2\pi]$) and a constant ($x_N \in [0, 1]$) generated from a uniform distribution in order to construct a uniformly distributed rotation matrix, as described in detail in Appendix B.

Finally, a deviation matrix $[\delta D]$ was added to the rotated marker-cluster $[R][A]$ to simulate a non-rigid deformation. $[\delta D]$ is a $N \times 3$ matrix that is made up of one single uniformly distributed randomly generated element $\delta d_{1,1} \in [-50, 50]$, with the rest of the elements equal to 0. Therefore, one single marker can

deviate up to 50 mm from its original position along the x-axis. The reason for this design was to obtain a uniformly distributed deviation magnitude across all the samples. Here the deformation magnitude is calculated as the matrix Frobenius norm of the deviation matrix, $\|\delta D\|$. In a typical MSFM segment, the major source of deformation would be soft tissue artefact (STA), measured by Kessler et al. (2019) to be up to 4.78 mm (at the first metatarsal base during running) and by Schallig et al. (2021) to be up to 9.3 mm (on the posterior aspect of the proximal calcaneus). In the thigh region, artefacts of up to 28.4 mm have been found during walking (Akbarshahi et al., 2010; Cereatti et al., 2017). Therefore, the choice of up to 50 mm covers the maximum deviation magnitude resulting for any single marker in a realistic lower-limb modelling scenario, not just at the foot. As $[A]$ is already a randomly generated configuration, the direction of the deviation does not have to be randomised. After steps 1–3 in Table 1 are completed, σ_{RBE} is computed (steps 4–5).

The variables examined here were not limited to the raw inputs to the model ($[A]$, $[B]$, $[\delta D]$, and $[R]$), and those that characterise the geometrical distribution of $[A]$ with a known influence on σ_{RBE} (Dorst, 2005). For example, although the segment size (S) is not a direct input to the model, it is a physical

Table 2. Descriptive statistics of the input parameters chosen for Monte-Carlo sampling.

Notation	Description	Unit	Range	Mean (S.D.)	Distribution
$\ \delta D\ $	Deformation magnitude	mm	[0.008, 49.999]	25.21 (14.52)	Uniform
a_{11}	Raw configuration elemental coordinate	mm	[−249.7, 249.9]	1.2 (146.1)	Uniform
β_N	Input for rotation matrix	rad	[0.00, 6.28]	3.15 (1.81)	Uniform
γ_N	Input for rotation matrix	rad	[0.00, 6.28]	3.12 (1.81)	Uniform
x_N	Input for rotation matrix	–	[0.00, 1.00]	0.50 (0.29)	Uniform

Note that only the first element of the marker configuration matrix $[A]$ is listed on the table for reference.

Table 3. Descriptive statistics of the output variables found by Monte-Carlo sampling.

Notation	Description	Unit	Range	Mean (S.D.)
σ_{RBE}	Rigid body error	mm	[0.001, 17.47]	7.05 (4.31)
R_{err}	Rotation error	–	[0, 1.92]	0.100 (0.101)
S	Segment size	mm	[58.76, 332.63]	203.15 (39.55)
kA	Condition number	1/mm	[0.002, 0.026]	0.005 (0.002)

characteristic of the marker-cluster that may reveal important information when interpreting the sensitivity of the input variables. Another variable examined in this study was the absolute condition number kA , which is indicative of the condition of the geometrical distribution the marker-cluster (Söderkvist and Wedin, 1994). For example, an ill conditioned problem that results in a badly estimated transformation matrix $[T]$ would be if a marker-cluster distributes all its landmarks on a straight line. Finally, the association of the rotation error (R_{err}) with each input variable was also investigated. The R_{err} measures the difference between $[R]$ and $[T]$, which indicates the quality of the shape alignment. (See Table 1, steps 6–8.)

2.3. Uncertainty, sensitivity analysis, and regression model

Six parameters were examined in this sensitivity analysis, including the direct input variables ($\|\delta D\|_N, \beta_N, \gamma_N, x_N$) and the variables with possible associations (S and kA). With the transformation matrix being the key variable associated with marker-cluster rigidity, the sensitivity of R_{err} to the input variables was evaluated against the input variables. The sensitivity of the input variables was quantified using the Pearson's correlation coefficient R , R^2 and the Spearman's ρ , due to their ease of computation and effectiveness in ranking the sensitivity amongst input parameters (Gardner et al., 1981). In addition, scatter-plots were used as they provide an immediate visual depiction of the relationship between the output and the input variables. An uncertainty analysis was conducted to validate the generated input parameters as well as to estimate the uncertainty of the outputs based on the samples generated.

To estimate σ_{RBE} based on the input variables here, a regression model was considered. Initially, to simplify the regression model, a sensitivity analysis was conducted to identify non-sensitive variables, that is, variables not correlated to σ_{RBE} . Based on the relationship between sensitive variables only and the σ_{RBE} , an appropriate regression model was proposed and its parameters estimated using a least squares approximation. In the situation where the relationship between the dependent and the independent variables was not linear, curvilinear regression or data transformation was applied. All statistical calculations were completed using SPSS (v24, IBM Corp., Armonk, USA).

3. Results

3.1. Uncertainty analysis

The spread of both input and output variables appeared to be within the expected range and distribution, both statistically (Tables 2 and 3) and visually from the probability density functions (Figures 1 and 2). Figure 2 also revealed that the segment size matched a normal distribution, and R_{err} and kA appeared to match a lognormal distribution. The distribution of the $\|\delta D\|$ followed a uniform distribution. However, differing from our expectation, σ_{RBE} did not follow a uniform distribution, but was skewed towards the lower values. Based on a mean deformation magnitude of 25.21 ± 14.52 mm, the corresponding σ_{RBE} was estimated to be 7.05 ± 4.31 mm.

3.2. Sensitivity analysis

Spearman's ρ was used as the primary measure of sensitivity rather than Pearson's R due to the possible

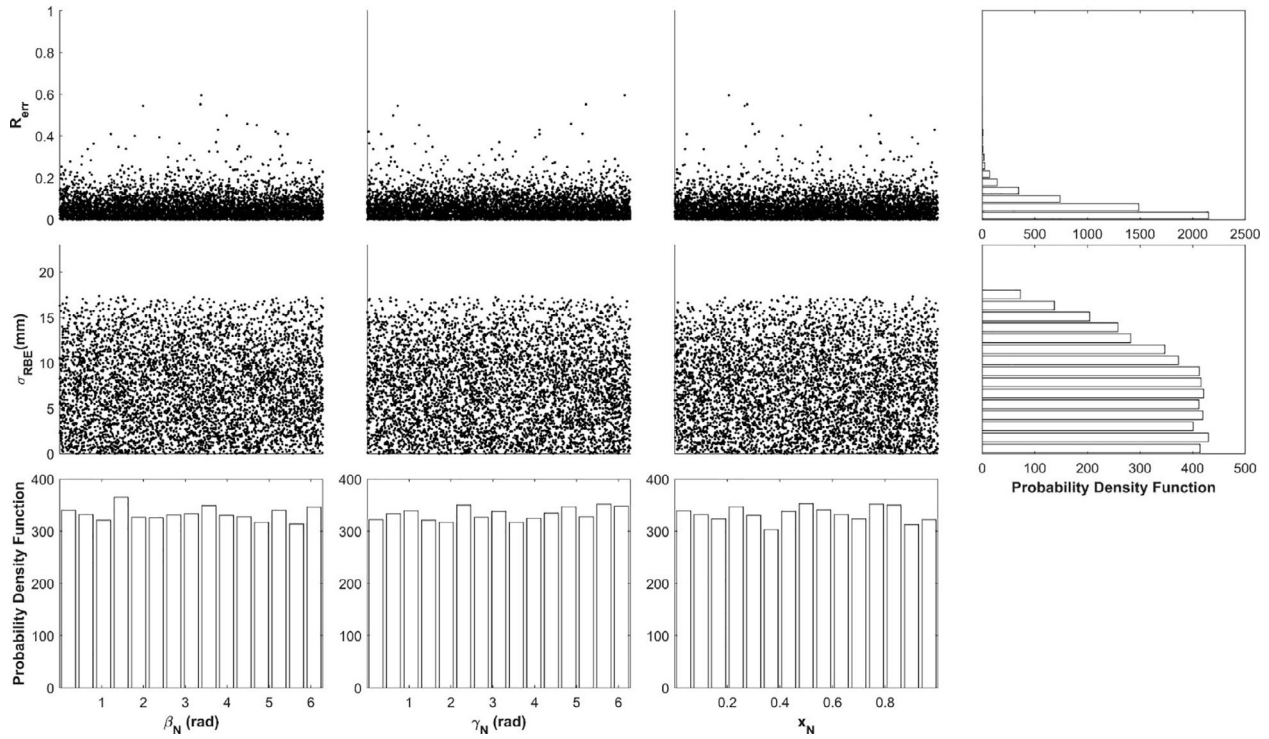


Figure 1. Scatter plot of rotation error (R_{err}) and rigid body error (σ_{RBE}) against the three rotation matrix inputs, β_N , γ_N , and x_N . The bottom and right most columns show the probability density function of the corresponding output generated by Monte Carlo sampling ($N = 5000$).

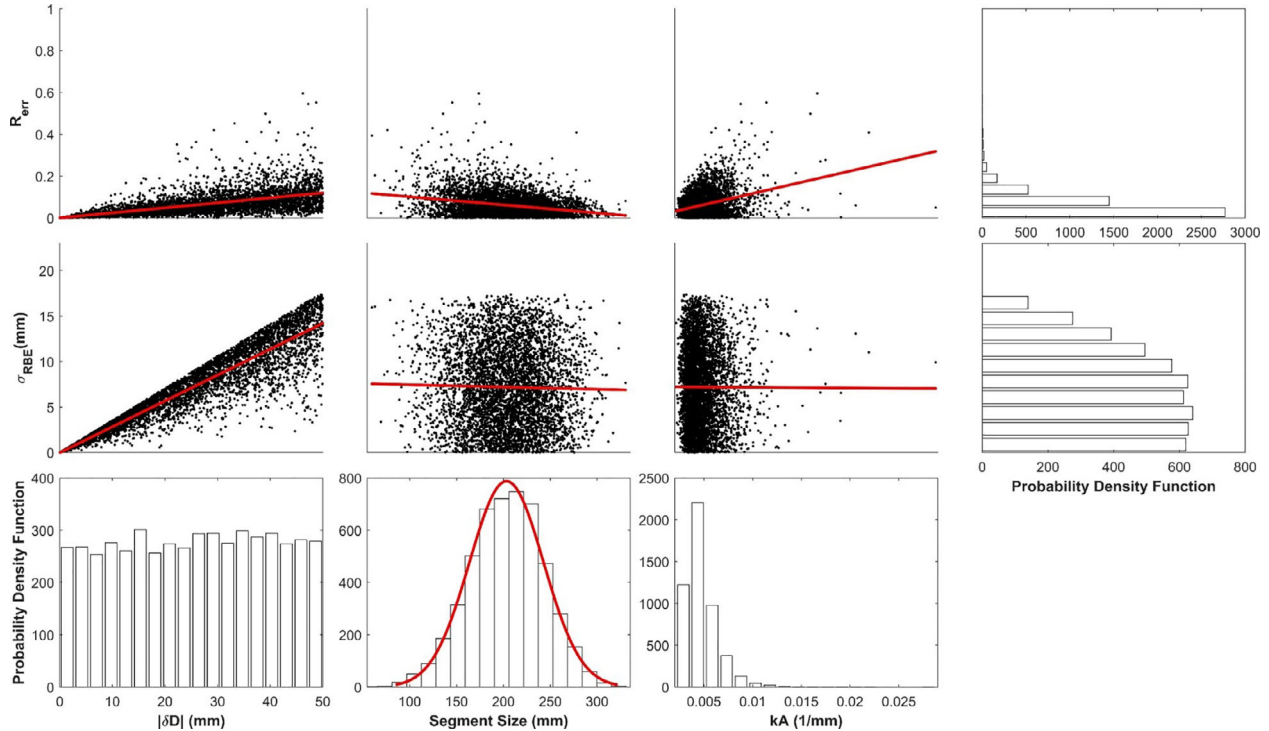


Figure 2. Scatter plot of rotation error (R_{err}) and rigid body error (σ_{RBE}) against deviation magnitude ($\|\delta D\|$), segment size, and condition number (kA). The bottom and right most columns show the probability density function of the corresponding output generated by Monte Carlo sampling ($N = 5000$).

non-linearity between σ_{RBE} and the input variables. The results indicate that the deformation magnitude $\|\delta D\|$ was the most dominant factor

influencing the variability of the σ_{RBE} (Table 4). The correlation coefficients suggest that the relation between $\|\delta D\|$ is highly linear ($R = 0.9311$) and highly

Table 4. Sensitivity indices for the σ_{RBE} estimated by Monte Carlo sampling ($N=5000$).

Sensitivity Parameter	Unit	Pearson's R	Spearman's ρ	R^2
$\ \delta D\ $	mm	0.9311*	0.9393*	0.8670
S	mm	-0.0091	-0.0008	0.0001
kA	(1/mm)	0.0078	0.0098	0.0001
β_N	Rad	0.0155	0.0159	0.0002
γ_N	Rad	0.0127	0.0074	0.0002
x_N	Rad	0.0086	0.0067	0.0001
Sum	—	—	—	0.8677

* p -value < 0.01**Table 5.** Sensitivity indices for the R_{err} estimated by Monte Carlo sampling ($N=5000$).

Sensitivity parameter	Unit	Pearson's R	Spearman's ρ	R^2
$\ \delta D\ $	mm	0.5968*	0.7494*	0.3561
S	mm	-0.2532*	-0.2247*	0.0642
kA	(1/mm)	0.3337*	0.2256*	0.1113
β_N	Rad	-0.0294*	-0.0077*	0.0009
γ_N	Rad	-0.0075	-0.0003	0.0001
x_N	Rad	0.0053	0.0029	0.0000
Sum	—	—	—	0.5326

* p -value < 0.01**Table 6.** Coefficients of the σ_{RBE} regression model.

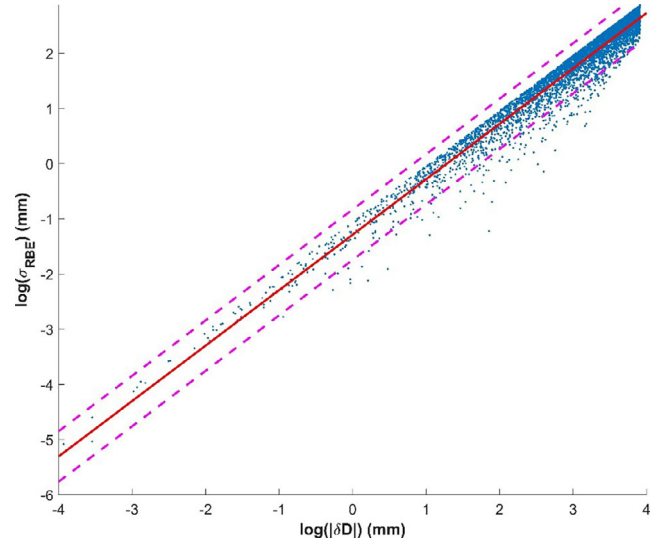
Term	Estimate	Std. Error	95% CI		t Stats	p-value
			Lower	Upper		
ζ_0	-1.288	0.009	-1.308	-1.270	-141.1	0.000
ζ_1	1.004	0.003	0.998	1.010	336.0	0.000

monotonic ($\rho=0.9393$). The sum of R^2 of all the sensitivity variables listed in Table 4 indicates that 86.77% of the σ_{RBE} variance is accounted for in this analysis, of which 86.70% is due to $\|\delta D\|$ alone. Apart from $\|\delta D\|$, none of the other variables ($\beta_N, \gamma_N, x_N, kA, S$) appear to have any significant influence on or association with σ_{RBE} .

The relationships between the inputs and the σ_{RBE} were also visualised using scatter plots as shown in Figures 1 and 2. Only $\|\delta D\|$ appears to have a strong relationship with σ_{RBE} , as indicated by the high concentration of data points along the upward sloped line of best-fit. R_{err} was also plotted against the input variables and kA , as it indicates the quality of the transformation matrix fitting, hence affecting the accuracy of quantifying rigidity using σ_{RBE} . As expected, there seems to be no effect of the rotation matrix inputs (Figure 1). However, a higher R_{err} appeared to be associated with samples with a higher $\|\delta D\|$, a smaller S , and a higher kA , with a ρ value of 0.7494, -0.2247, and 0.2256 respectively (Table 5).

3.3. Regression model

The input variables were first screened based on the result of the sensitivity analysis, where all but one of the input variables were eliminated due to their weak

**Figure 3.** Fitted plot of $\log(\sigma_{RBE})$ vs $\log(\|\delta D\|)$, with a line of best-fit (solid line) and a 95% confidence interval (dotted line).

correlation with σ_{RBE} (Table 4). The fact that only $\|\delta D\|$ showed a highly linear and monotonic relationship with the σ_{RBE} means that the regression model can be greatly simplified. However, the scatter plot (Figure 2) clearly indicates a violation of homoscedasticity (where the variances along the line of best fit increase with $\|\delta D\|$); Therefore, a data transformation is required to reduce this effect. Here, both the $\|\delta D\|$ and σ_{RBE} were log (natural logarithm) transformed, and their functional relationship was expressed as a linear equation:

$$\log(\sigma_{RBE}) = \zeta_0 + \zeta_1 \log(\|\delta D\|) + \epsilon \quad (2)$$

where ζ_0 is the intercept, ζ_1 the slope of the line, and ϵ the random error. The fitted model is shown in Figure 3, with the model coefficients in Table 6.

Analysis of variance of the regression model suggested that there is a linear association between the natural logarithm of the $\|\delta D\|$ and the natural logarithm of the σ_{RBE} ($p < 0.01$). In addition, the obtained R^2 and adjusted $R^2 = 0.944$ indicated that the model can explain 94% of the variation in the σ_{RBE} . Furthermore, both ζ_0 and ζ_1 were significant ($p < 0.01$), showing that the model $\log(\sigma_{RBE}) = -1.288 + 1.004 \log(\|\delta D\|)$ is appropriate to describe the relationship between $\|\delta D\|$ and σ_{RBE} . In terms of the effects of changes in $\|\delta D\|$ on σ_{RBE} , with a value of ζ_1 equal to 1.004, this means that a 10% increase in the $\|\delta D\|$ would lead to a 10.04% increase in σ_{RBE} .

4. Discussion

There is a lack of consensus on how the foot should be tracked or represented in MSFMs used in clinical

gait analysis. An earlier study by Chan et al. (2019) concerning the rigidity of the hindfoot, forefoot, and tibia segment suggested that the forefoot is the least rigid segment and questioned its rigid body assumption. Similar methods of utilising transformation residuals to compute marker-cluster rigidity were also used in previous studies to quantify the non-rigid motion of the soft tissue artefacts (van den Bogert et al., 1994; Grimpampi et al., 2014). To date, there has not been a study of the efficacy of using σ_{RBE} to quantify rigidity. In this paper, Monte-Carlo based techniques were utilised to conduct a GSA and a UA to determine whether σ_{RBE} is a suitable measure to quantify the rigidity of a generic MSFM segment tracked using a four marker cluster. The GSA confirmed that that σ_{RBE} is most sensitive to deformation magnitude $\|\delta D\|$ compared to all other variables. Furthermore, the RA confirmed that σ_{RBE} is associated linearly with $\|\delta D\|$, which suggests that the σ_{RBE} is an appropriate measure of marker-cluster deformation. Therefore, this study provides the evidence to support the use of σ_{RBE} to compute and compare marker-cluster rigidity in MSFMs (or in any similarly sized body segments tracked with four skin-mounted markers).

The main objective of the GSA was to identify the most critical variables that influence the output through obtaining a ranking of the input variables using a specific ‘importance’ or ‘sensitivity’ index (Pannell, 1997). Hamby (1994) outlined fourteen possible sensitivity indices for cases where only a single output variable is to be evaluated, and Saltelli et al. (1993) reviewed a total of fifteen. Although the baseline strategy for conducting a global sensitivity analysis has already been established in the literature, the result may be different depending on the techniques used (OAT, Monte-Carlo, FAST, etc.) and the indices that rank the variables. In this analysis, R and Spearman’s ρ were used to rank and compare the sensitivity of the variables as the coefficients can be easily computed and are effective in ranking sensitivity (Gardner et al., 1981; Saltelli et al., 2007). Since linearity cannot be assumed between the input variables and the σ_{RBE} , Spearman’s ρ was chosen to be the main factor in ranking the sensitivity.

The reference marker-cluster configurations $[A]$ were generated randomly to represent a range of different geometries. In marker based MSFMs, segments are defined in many different ways and the tracking markers therefore can be in a variety of arrangements (Rankine et al., 2008; Deschamps et al., 2011). The Monte Carlo method of generation creates good

geometries as well as bad ones (i.e. abnormal shapes that do not realistically represent a segment) to be included in both uncertainty and sensitivity analyses, resulting in an underestimation of the variable sensitivity and model accuracy.

Söderkvist and Wedin (1993) have shown that the quality of the transformation matrix fitting depends on the reference landmark configuration. The problem of determining the rotation matrix can be very ill conditioned when the singular values of $[A]$ are very small, e.g. when markers are almost in a straight line. Therefore, when quantifying the rigidity of an MSFM segment, it is also important to make sure that the marker distribution will not result in a poor determination of the transformation matrix $[T]$ (equation 1). This can be achieved by estimating the R_{err} and kA of a particular configuration.

This study was designed to study the relationship between the variables contributing to marker-cluster deformation and σ_{RBE} , and there are several factors that must be considered when interpreting results. Firstly, the translation element was not included for two reasons. The translation vector of $[T]$ is determined in the final step of the computation and therefore also depends on R_{err} . Therefore, any errors quantified by R_{err} will propagate to the translation vector. In addition, the distance between $[A]$ and $[B]$ does not influence the calculation of the σ_{RBE} , as one can simply force the two configurations to coincide at their geometric centroid by applying a rigid translation. Secondly, deformation has only been applied to one single marker. The focus of this study has been to investigate the correlation between the applied deformation magnitude $\|\delta D\|$ with σ_{RBE} . With this in mind, the experiment was designed to generate a uniformly distributed $\|\delta D\|$, which is not possible when introducing perturbations in multiple markers at the same time. Finally, the UA and GSA were performed only on clusters of four markers. Further investigation is required to assess the relationship between the deformation and σ_{RBE} in segments composed of different numbers of markers. Adding more markers on the small foot segments is likely to be impractical but would increase the accuracy of determining the transformation matrix (Söderkvist and Wedin, 1993).

To show that σ_{RBE} can be used to quantify rigidity, a simple linear regression analysis was conducted to provide evidence for the relationship between σ_{RBE} and the simulated deformation magnitude $\|\delta D\|$. The least square approximation of the regression model parameters showed a strong significance, thus providing a strong case for using the proposed equation to

model σ_{RBE} . However, a gap between the upper bound of the prediction interval and the actual data indicates that the variance is skewed towards the lower bound (Figure 3). Furthermore, despite effort to reduce the heterogeneity of the data through a log-log transformation, the problem of homoscedasticity still exists. Although homoscedasticity does not cause bias in the estimate of the regression model parameters (Rawlings et al., 1998), it will likely underestimate the variance of the σ_{RBE} at a large $\|\delta D\|$ and overestimate the variance at a small $\|\delta D\|$. Finally, some outliers were also observed at the bottom right of the line of best fit, which could also potentially impact the estimation of the model parameters. Overall, it is noted that a better regression model is needed if the primary goal is to predict the specific value and variance of the σ_{RBE} . Nevertheless, the regression model still clearly indicates a strong and predicatable relationship between σ_{RBE} and $\|\delta D\|$.

5. Conclusion

A Monte-Carlo based GSA has been successfully applied to show that the deformation magnitude $\|\delta D\|$ is the most sensitive variable of the σ_{RBE} out of all that were assessed in this study, and that it accounts for 86.7% of the total variation. The GSA further showed that the σ_{RBE} does not depend on the segment size and rotational motion. However, the geometric distribution of the markers appeared to have an effect on the computation of the σ_{RBE} . Nevertheless, the highly linear and monotonic relationship between the σ_{RBE} and $\|\delta D\|$, along with the proposed linear regression model, suggests that σ_{RBE} can be used to quantify segment rigidity and deformation caused by either bone motion or soft tissue artefact in a MSFM segment tracked using four markers.

Disclosure statement

The authors declare that there are no conflicts of interest in the present study.

References

- Akbarshahi M, Schache AG, Fernandez JW, Baker R, Banks S, Pandy MG. 2010. Non-invasive assessment of soft-tissue artifact and its effect on knee joint kinematics during functional activity. *J Biomech.* 43(7):1292–1301.
- Arvo J. 1992. Fast random rotation matrices. in: *Graphics Gems III*. San Diego, CA: Academic Press, p. 117–120.
- Ata MY. 2007. A convergence criterion for the Monte Carlo estimates. *Simul. Model. Pract. Theory.* 15(3): 237–246.
- Bathe K. 2014. *Finite element procedures*, 2nd ed. Watertown, MA: Klaus-Jürgen Bathe.
- Bruening DA, Cooney KM, Buczek FL. 2012. Analysis of a kinetic multi-segment foot model. Part I: Model repeatability and kinematic validity. *Gait Posture.* 35(4): 529–534.
- Cereatti A, Bonci T, Akbarshahi M, Aminian K, Barré A, Begon M, Benoit DL, Charbonnier C, Dal Maso F, Fantozzi S, et al. 2017. Standardization proposal of soft tissue artefact description for data sharing in human motion measurements. *J Biomech.* 62:5–13.
- Chan P-H, Stebbins J, Zavatsky AB. 2019. Marker cluster rigidity in a multi-segment foot model. *J Biomech.* 84: 284–289.
- Deschamps K, Staes F, Roosen P, Nobels F, Desloovere K, Bruyninckx H, Matricali GA. 2011. Body of evidence supporting the clinical use of 3D multisegment foot models: A systematic review. *Gait Posture.* 33(3): 338–349.
- DiLiberto FE, Tome J, Baumhauer JF, Houck J, Nawoczenski DA. 2015. Individual metatarsal and forefoot kinematics during walking in people with diabetes mellitus and peripheral neuropathy. *Gait Posture.* 42(4): 435–441.
- Dorst L. 2005. First order error propagation of the Procrustes method for 3D attitude estimation. *IEEE Trans Pattern Anal Mach Intell.* 27(2):221–229.
- Gardner RH, O'Neill RV, Mankin JB, Carney JH. 1981. A comparison of sensitivity analysis and error analysis based on a stream ecosystem model. *Ecol. Modell.* 12(3): 173–190.
- Green BF. 1951. The orthogonal approximation of an oblique structure in factor analysis. *ETS Res. Bull. Ser.* 1951(2):1–11.
- Grimpampi E, Camomilla V, Cereatti A, De Leva P, Cappozzo A. 2014. Metrics for describing soft-tissue artefact and its effect on pose, size, and shape of marker clusters. *IEEE Trans Biomed Eng.* 61(2):362–367.
- Hamby DM. 1994. A review of techniques for parameter sensitivity analysis of environmental models. *Environ Monit Assess.* 32(2):135–154.
- Hanson RJ, Norris MJ. 1981. Analysis of measurements based on the singular value decomposition. *SIAM J Sci Stat Comput.* 2(3):363–373.
- Iooss B, Lemaître P. 2015. A review on global sensitivity analysis methods. in: *Uncertainty management in simulation-optimization of complex systems*. New York: Springer, p. 101–122.
- Kessler SE, Rainbow MJ, Lichtwark GA, Cresswell AG, D'Andrea SE, Konow N, Kelly LA. 2019. A direct comparison of biplanar videoradiography and optical motion capture for foot and ankle kinematics. *Front Bioeng Biotechnol.* 7:199.
- Law AM, Kelton WD. 1982. Confidence intervals for steady-state simulations II: A survey of sequential procedures. *Manage. Sci.* 28(5):550–562.
- Law AM, Kelton WD. 1984. Confidence intervals for steady-state simulations: I. A survey of fixed sample size procedures. *Oper. Res.* 32(6):1221–1239.
- Leardini A, Caravaggi P, Theologis T, Stebbins J. 2019. Multi-segment foot models and their use in clinical populations. *Gait Posture.* 69:50–59.

- Leardini A, Chiari L, Della Croce U, Cappozzo A. 2005. Human movement analysis using stereophotogrammetry. Part 3. Soft tissue artifact assessment and compensation. *Gait Posture*. 21(2):212–225.
- Leitch J, Stebbins J, Zavatsky AB. 2010. Subject-specific axes of the ankle joint complex. *J Biomech*. 43(15): 2923–2928.
- Nester CJ, Liu AM, Ward E, Howard D, Cocheba J, Derrick T. 2010. Error in the description of foot kinematics due to violation of rigid body assumptions. *J Biomech*. 43(4):666–672.
- Pannell DJ. 1997. Sensitivity analysis of normative economic models: Theoretical framework and practical strategies. *J. Agric. Econ.* 16(2):139–152.
- Pothrat C, Authier G, Viehweger E, Berton E, Rao G. 2015. One- and multi-segment foot models lead to opposite results on ankle joint kinematics during gait: Implications for clinical assessment. *Clin Biomech (Bristol, Avon)*. 30(5):493–499.
- Rankine L, Long J, Canseco K, Harris G. 2008. Multisegmental foot modeling: a review. *Crit Rev Biomed Eng*. 36(2–3):127–181.
- Rawlings JO, Pantula SG, Dickey DA. 1998. *Applied regression analysis*, 2nd ed. New York: Springer.
- Rouhani H, Favre J, Crevoisier X, Jolles BM, Aminian K. 2011. Segmentation of foot and ankle complex based on kinematic criteria. *Comput Methods Biomech Biomed Engin.* 14(9):773–781.
- Saltelli A, Andres TH, Homma T. 1993. Sensitivity analysis of model output: An investigation of new techniques. *Comput. Stat. Data Anal.* 15(2):211–238.
- Saltelli A, Ratto M, Andres T, Campolongo F, Cariboni J, Gatelli D, Saisana M, Tarantola S. 2007. *Global sensitivity analysis. The primer*. John Wiley & Sons, Ltd, Chichester, UK.
- Sawacha Z, Gabriella G, Cristoferi G, Guiotto A, Avogaro A, Cobelli C. 2009. Diabetic gait and posture abnormalities: A biomechanical investigation through three dimensional gait analysis. *Clin Biomech (Bristol, Avon)*. 24(9): 722–728.
- Schallig W, Streekstra GJ, Hulshof CM, Kleipool RP, Dobbe JGG, Maas M, Harlaar J, Krogt MM, Van Der Noort JC. Van Den 2021. The influence of soft tissue artifacts on multi-segment foot kinematics. *J Biomech*. 120:110359.
- Schönemann PH. 1966. A generalized solution of the orthogonal Procrustes problem. *Psychometrika*. 31(1): 1–10.
- Söderkvist I, Wedin PÅ. 1993. Determining the movements of the skeleton using well-configured markers. *J Biomech*. 26(12):1473–1477.
- Söderkvist I, Wedin PÅ. 1994. On condition numbers and algorithms for determining a rigid body movement. *Bit*. 34(3):424–436.
- Spoor CW, Veldpaus FE. 1980. Rigid body motion calculated from spatial co-ordinates of markers. *J Biomech*. 13(4):391–393.
- Theologis T, Stebbins J. 2010. The use of gait analysis in the treatment of pediatric foot and ankle disorders. *Foot Ankle Clin.* 15(2):365–382.
- Turner DE, Woodburn J. 2008. Characterising the clinical and biomechanical features of severely deformed feet in rheumatoid arthritis. *Gait Posture*. 28(4):574–580.
- van den Bogert AJ, Smith GD, Nigg BM. 1994. In vivo determination of the anatomical axes of the ankle joint complex: An optimization approach. *J Biomech*. 27(12): 1477–1488.
- Wolf P, Stacoff A, Liu A, Nester C, Arndt A, Lundberg A, Stuessi E. 2008. Functional units of the human foot. *Gait Posture*. 28(3):434–441.

Appendix A: Convergence assessment of the Monte-Carlo simulation

Monte-Carlo based sensitivity analysis is a numerical procedure that estimates the descriptive statistics and the sensitivity parameters. Naturally the accuracy and stability of the estimates depends on the sample size or the stopping rule imposed on each Monte-Carlo iteration, and there are various methods to achieve this. Similar to how a convergence assessment is usually conducted in a finite-element analysis (Bathe, 2014), one can increase the sample size until any addition no longer changes the accuracy of the result. Alternatively, the rate of convergence can be determined through visual inspection or more objectively by a defined criteria, usually by a confidence interval (Law and Kelton, 1984, 1982). In this study, the convergence criteria will be determined using the method proposed by Ata (2007) that calculates a convergence band of a predefined length and width that changes for every iteration. The convergence band length and band width act as an exit condition for the loop that determines the accuracy of the steady-state mean. This is also termed the acceptable shifting convergence band rule (ASCB) and can be easily embedded within the Monte Carlo algorithm as a stopping rule for the while loop.

In ASCB, the convergence of a parameter is detected when its mean is stable within a defined convergence band (CB) width ($2\epsilon^*$) over a number of samples (CB length ζ^*) generated by the Monte-Carlo algorithm. At the start of the code, the algorithm requires the definition of the convergence band half-width (ϵ^*) and length (ζ^*). Let X be a random variable (e.g. $|\delta B|_i$) with the distribution $\sigma_{RBE}(X)$ and x_i the random sample from $F(X)$. This algorithm begins by calculating the mean of the Monte-Carlo samples consisting of all the observations from the 1st to the j^{th} , the current trial:

$$\bar{x}_j = \frac{1}{j} \sum_{i=1}^j x_i \quad (A1)$$

For each loop, the algorithm assesses whether adding one extra sample x_j will result in a significant change in the mean such that it falls outside the current CB width, where the upper bound $U(\bar{x}_{j-1})$ and lower bound $L(\bar{x}_{j-1})$ of the previous iteration are defined as:

$$\begin{aligned} U(\bar{x}_{j-1}) &= \bar{x}_{j-1} + \epsilon^*; \\ L(\bar{x}_{j-1}) &= \bar{x}_{j-1} - \epsilon^* \end{aligned} \quad (A2)$$

If the new mean \bar{x}_j falls outside these bounds, the CB width will be redefined; otherwise the band remains the same as:

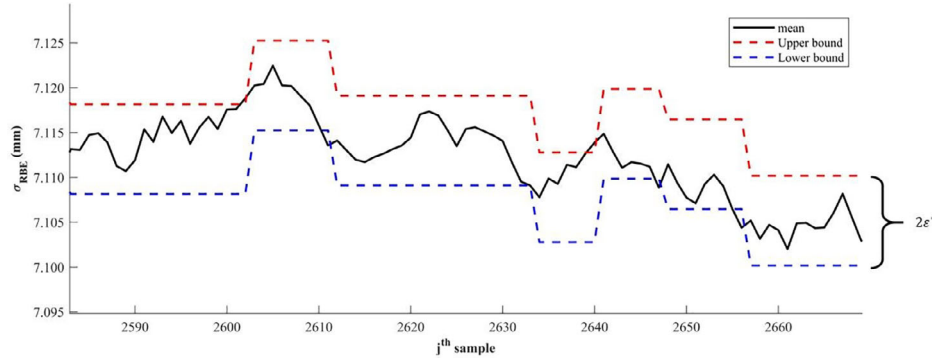


Figure A1. Example of a shifting convergence band as the mean falls outside the existing limits.

Table A1. Parameters tested in the Monte-Carlo convergence assessment.

Notation	Type	Description	Unit	Resolution	CB half width (ϵ^*)
σ_{RBE}	Output	Rigid body error	mm	0.01	0.005
S	Output	Segment size	mm	0.1	0.05
kA	Output	Condition number	1/mm	0.0001	0.00005
$Rerr$	Output	Rotation Error	—	0.001	0.0005
$ \delta D $	Input	Deformation magnitude	mm	0.1	0.05
α_N	Input	Input for rotation matrix	rad	0.01	0.005
β_N	Input	Input for rotation matrix	rad	0.01	0.005
χ_N	Input	Input for rotation matrix	—	0.01	0.005

Table A2. Convergence size obtained by the ASCBR algorithm.

Notation	Unit	Required Resolution	Converged mean (Standard deviation)	Convergence sample size
σ_{RBE}	mm	0.01	7.32 (4.42)	2747
$ \delta D $	mm	0.1	25.1 (14.4)	1349
S	mm	0.1	203.9 (39.2)	3197
kA	1/mm	0.0001	0.0047 (0.0016)	191
$Rerr$	—	0.001	0.061 (0.061)	468
α_N	Rad	0.01	3.14 (1.81)	370
β_N	Rad	0.01	3.17 (1.81)	302
χ_N	—	0.01	0.51 (0.29)	350

$$U(\bar{x}_j) = \begin{cases} U(\bar{x}_{j-1}), \delta_j = 0, \\ \bar{x}_j + \epsilon^*, \delta_j = 1, \end{cases}$$

and

$$L(\bar{x}_j) = \begin{cases} L(\bar{x}_{j-1}), \delta_j = 0, \\ \bar{x}_j - \epsilon^*, \delta_j = 1, \end{cases} \quad (A3)$$

where

$$\delta_j = \begin{cases} 0, & L(\bar{x}_{j-1}) < \bar{x}_j < U(\bar{x}_{j-1}), \\ 1, & \{\bar{x}_j \leq L(\bar{x}_{j-1})\} \vee \{\bar{x}_j \geq U(\bar{x}_{j-1})\}. \end{cases} \quad (A4)$$

The number of adjacent sample means, which share the same upper and lower band limits as defined in (3), i.e. $\delta = 0$ for all of them, is recorded as:

$$Z_j = \begin{cases} Z_j + 1, & \delta_j = 0, \\ 0, & \delta_j = 1. \end{cases} \quad (A5)$$

for every loop. Once Z_j reaches the required CB length (ζ^*) the algorithm terminates and concludes that convergence is reached according to the specified band width. Figure A1 shows an example of a section of the ASCBR code output embedded within the Monte-Carlo simulation conducted for this sensitivity study. When the mean falls outside the CB width, the algorithm takes into account the all the

existing samples and redefines a new CB. The loop will only end when the mean stays within the CM over a pre-defined length.

In this paper, the CB width (half the resolution) was defined according to the resolution specified in Table A1. The CB length was defined as 50 iterations, which is suggested in the literature (Ata, 2007) as the optimal length. The ASCBR algorithm was embedded within the Monte-Carlo experiment written in MATLAB (v2015a, MathWorks Inc., Natick, USA), described in Section 2.2.

The required resolution and the number of samples required to meet the target for each parameter are listed in Table A2. The result of this assessment suggests that the sample size for this Monte-Carlo based global sensitivity analysis should be a minimum of 3197.

Appendix B: Random rotation matrix generation for Monte-Carlo sampling

The simplest and most intuitive method of generating a random rotation matrix that covers all possible angles is by choosing three random Euler angles α , β , and γ , each from a uniform distribution, followed by the computation of the rotation matrix through multiplying the three elemental

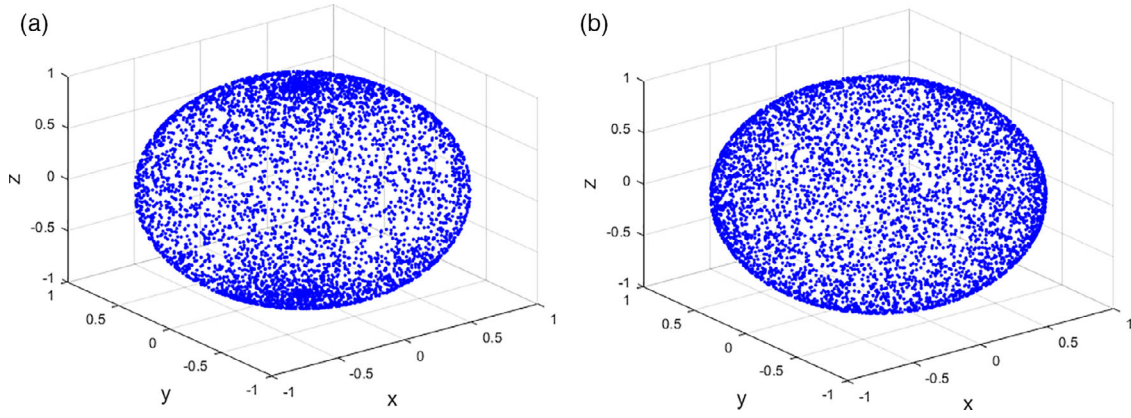


Figure B1. Random rotation matrix distribution using (a) sequential elemental rotation matrices and (b) solution proposed by Arvo (1992).

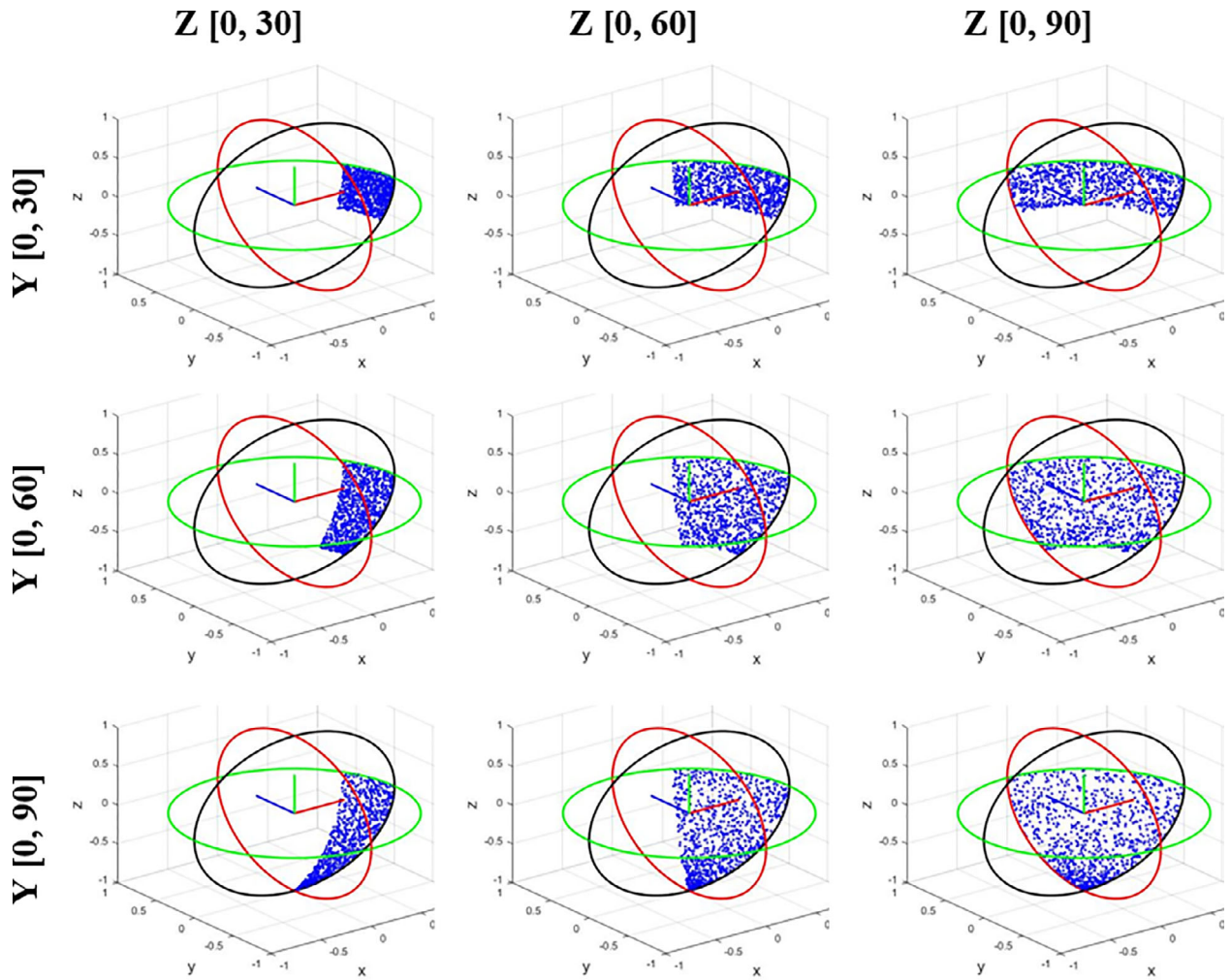


Figure B2. Demonstration of random rotation matrix distribution using sequential elemental rotation matrices based on Z-Y-X Euler convention, where both Z and Y angles are generated based on a uniform distribution. From left to right column: Increasing Z angle range; From top to bottom: Increasing Y angle range.

rotation matrices. However, this method will not result in a rotation matrix that is uniformly distributed (Figure B1 a).

In Figure B1 a) a vector $k = (1, 0, 0)$ is rotated 5000 times using a rotation matrix (Euler Z-Y-X convention) generated by the sequential elemental rotation matrices, where

individual Euler angles are sampled from a uniform distribution over $[0, 2\pi]$. A higher density of points around the poles (where the z-coordinate takes a value closer to either 1 or -1) can be observed in the figure, demonstrating non-uniformity of the rotation being generated. This effect

can be seen more clearly when we limit the range of rotation angle as shown in Figure B2. For the vector $k = (100)$, the longitude position of the rotated point depends on the Z angle whereas the position along the latitude depends on the Y angle. With increasing Y angle towards the poles, the points tend to be more concentrated as the circumference of the latitude becomes smaller.

Instead of generating rotation by three consecutive random angles, Arvo (1992) utilised a random reflection after the first rotation to produce a truly random rotation (Figure B1 b). The first step involves a rotation of the position vector k about the z-axis:

$$R = \begin{bmatrix} \cos(\alpha_N) & \sin(\alpha_N) & 0 \\ -\sin(\alpha_N) & \cos(\alpha_N) & 0 \\ 0 & 0 & 1 \end{bmatrix} \quad (\text{B1})$$

The second step involves the calculation of a Householder reflection:

$$H = I - 2vv^T \quad (\text{B2})$$

The reflection moves k to another point p on the sphere via a reflection through the hyperplane that is orthogonal to the line \overline{kp} and containing the origin, where v is a unit vector parallel to the line \overline{kp} . In Arvo's method, the vector v is defined as:

$$v = \begin{bmatrix} \cos(\beta_N)\sqrt{x_N} \\ \sin(\beta_N)\sqrt{x_N} \\ \sqrt{1-x_N} \end{bmatrix} \quad (\text{B3})$$

where $\beta_N = [0, 2\pi]$ and $x_N = [0, 1]$. This method leads to points uniformly distributed across the surface of the sphere. If we take the initial point to be $= (100)$, then the rotated point p can be calculated as $p = Hz$ where p is defined as:

$$p = (I - 2vv^T)z = \begin{bmatrix} -2\cos(\beta_N)\sqrt{x_N(1-x_N)} \\ -2\sin(\beta_N)\sqrt{x_N(1-x_N)} \\ 2x_N - 1 \end{bmatrix} \quad (\text{B4})$$

The z-component of p is uniformly distributed over $[-1, 1]$, and the x and y-components of p are uniformly distributed over $[0, 2\pi]$, as required. In summary, Arvo's random rotation matrix is generated using three separate uniformly generated random inputs, two angles (α_N, β_N) and one constant, (x_N) . The first angle, α_N , describes the random rotation about its z-axis, and the second angle and a constant (β_N, x_N) describes the orientation of the randomly generated hyperplane that reflects the point anywhere on the sphere (Figure B1 b).